Progress In Electromagnetics Research C, Vol. 155, 121–126, 2025

PIER C

(Received 2 April 2025, Accepted 25 April 2025, Scheduled 5 May 2025)

Physics-Based 2D Direction Finding of an Amplitude Modulated Signal Using a Uniform Triangular Array

Kai Ren*

Department of Electrical Engineering and Computer Science, South Dakota School of Mines and Technology
Rapid City, SD 57701, USA

ABSTRACT: A uniform triangular array (UTA) is proposed for physics-based 2D direction-of-arrival (DOA) estimations of unknown incoming signals. Three capacitively loaded top-hat antennas are used as array elements. Unlike conventional array-based direction finding (DF) systems, complex antenna radiation patterns are used in array manifold calculations and DOA predictions, where coupling among array elements is naturally resolved. Both continuous wave (CW) signals and single tone signals with amplitude modulation (AM) are considered in DF simulations. Cramer-Rao bound (CRB) values are calculated to provide theoretical lower bounds of DF accuracies. Multiple signal classification (MUSIC) algorithm is used to further demonstrate the DF performance of the triangular antenna array without any angle ambiguities within the field of view from 0° to 360° in the azimuth direction and from 1.25° to 178.75° in the elevation direction.

1. INTRODUCTION

In the pursuit of enhancing navigation and communication systems, direction finding (DF) plays a vital role in both civil and military applications. In these DF systems, antenna arrays are crucial components for direction-of-arrival (DOA) estimations [1–7]. However, the presence of mutual coupling will deteriorate DF accuracies of conventional arrays. In communication and signal processing communities, various decoupling methods have been investigated to mitigate mutual coupling [3–7].

In [3], mutual coupling among antenna elements was modeled by a banded complex symmetric Toeplitz matrix and considered in DOA estimations. In [4] and [5], an over-complete block matrix based on the steering vector was constructed to mitigate the mutual coupling effect. In [6], rank-reduction theory was implemented to eliminate mutual coupling. In [7], mutual coupling effects were reduced by using sparse array configuration and increasing separations among elements. Different DF array geometries have been explored in reducing mutual coupling as well, such as uniform linear array (ULA) [3–5], uniform circular array (UCA) [6], sparse ULA [7], nonuniform linear array [8], and triangular array (TA) [9]. In achieving accurate DOA estimations, various modulated incident signals have been considered, such as linear frequency modulation (LFM) [9], amplitude modulation (AM) [10], frequency modulation (FM) [11], and binary phase shift keying (BPSK) [12]. However, these designs and corresponding algorithms did not consider practical antenna elements and radiation patterns. To investigate the impact of antennas on DF systems, realistic antenna elements were incorporated in [8, 13–15]. In [8], DOA estimations were achieved by considering mutual coupling through impedance matching of small, tuned dipole antennas in five-element uniform and nonuniform arrays. In [13–15], realized antenna gain patterns were implemented in DF algorithms to achieve accurate signal predictions. However, the incident waves were assumed to have constant amplitude values, and signal modulation was not considered. To the best of the author's knowledge, physics-based DOA estimations of incoming AM signals were not investigated based on UTA with considering antenna radiation patterns.

In this paper, a UTA using three top-hat antennas is proposed to achieve DOA estimations of incident narrow-band signals with different azimuth, elevation, and polarization angles. Unlike the conventional DF arrays [1–7, 9–12], a physics-based DF algorithm is applied to improve accuracies of DOA estimations, where the coupling among antenna elements is naturally considered by using complex radiation patterns rather than array factors. Unlike the traditional array elements using linear wire antennas with a narrow frequency bandwidth [1–12], wideband top-hat antennas are implemented to increase the possibility of detections and interceptions. Unlike the DF antennas considering gain patterns and assuming transmitted signals with a constant amplitude [13–15], DOA estimations are achieved based on incident CW and AM signals. As a design example, the proposed DF UTA operates at 650 MHz, which is scalable to any microwave frequency of interest. To improve the operation frequency bandwidth of the antenna, capacitively loaded top-hat antennas are used as the array elements. Both CRB values and MUSIC algorithm are implemented to demonstrate the DF capability of the proposed unambiguous UTA.

2. AMPLITUDE MODULATION AND PHYSICS-BASED MUSIC ALGORITHM

Figure 1 presents DF problem setup, where an incident CW or AM signal with an elevation angle of θ', an azimuth angle of ϕ',

* Corresponding author: Kai Ren (kai.ren@sdsmt.edu).

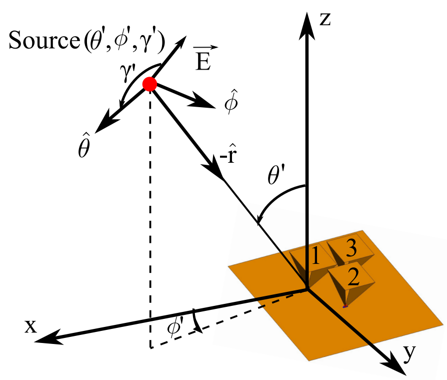

FIGURE 1. A uniform triangular array (UTA) is illuminated by a linearly polarized incoming plane wave with DOA of (θ', ϕ') and a polarization angle of γ'. The feeding point of the antenna element 1 is located at the origin.

and a polarization angle of γ' illuminates the UTA. The feeding point of the antenna element 1 is located at the origin. The UTA receiver is in the far field of the transmitter. The electric field intensity of a linearly polarized incident wave at the receiver can be expressed by [2],

$$\begin{aligned}\vec{E}(t) &= \hat{\phi}E_\phi(t) + \hat{\theta}E_\theta(t) \\ &= m(t)e^{j\omega_c t}e^{j\phi_c}[\hat{\phi}\sin(\gamma) + \hat{\theta}\cos(\gamma)]\end{aligned} \tag{1}$$

where $m(t)$ is the modulating or baseband signal; $\omega_c = 2\pi f_c$ is the angular frequency of the carrier signal; and the phase of the carrier signal is ϕ_c. For a CW signal, $m(t) = 1$, which is not a function of time. For a single tone modulating signal,

$$m(t) = A_c + A_m \cos(2\pi f_m t + \phi_m) \tag{2}$$

where the amplitude of the modulating signal is A_m; the amplitude of the carrier signal is A_c; the operating frequency of the modulating signal is f_m; and the phase of the modulating signal is ϕ_m. Fig. 2 shows the real component of the AM signal under the assumption that $A_m = A_c = 1$ and $\phi_m = \phi_c = 0$. Fig. 2 top is the modulating signal with $m(t) = 1 + \cos(2\pi f_m t)$ and $f_m = 20\,kHz$. Fig. 2 middle is the real component of the carrier signal $Re\{e^{j2\pi f_c t}\}$ with $f_c = 650$ MHz. Fig. 2 bottom is the corresponding real part of the AM signal $m(t)\cdot Re\{e^{j2\pi f_c t}\}$.

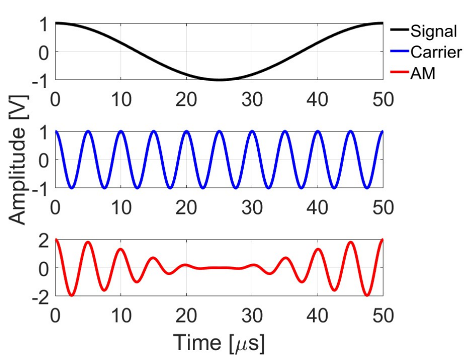

FIGURE 2. An amplitude modulated (AM) signal. Top: A single tone modulating signal at 20 kHz. Middle: A carrier signal at 650 MHz. Bottom: The corresponding AM signal.

Note that Fig. 2 middle can also be treated as a CW signal with $m(t) = 1$. The period of the carrier signal at 650 MHz is approximately 1.54 ns. To have a better observation on the carrier signal, a coarse sampling point of 571 is chosen to obtain Fig. 2.

The received voltage $v_n(t)$ of the source signal at the nth antenna ($n = 1$, 2, or 3) in the three-element UTA is given by,

$$v_n(t) = G_{n\phi}(\theta,\phi)E_\phi(t) + G_{n\theta}(\theta,\phi)E_\theta(t) + w_n(t) \tag{3}$$

where $G_{n\phi}(\theta,\phi)$ and $G_{n\theta}(\theta,\phi)$ are ϕ and θ components of the complex radiation pattern of the nth antenna element. $E_\phi(t)$ and $E_\theta(t)$ are ϕ and θ components of electrical field intensities of transmitted signals shown in (1). $w_n(t)$ is the Gaussian white noise. Unlike the conventional MUSIC algorithm [1], the practical radiation patterns are considered in the column vector Y, rather than the assumption of isotropic antennas. This leads to a physics-based MUSIC algorithm,

$$P_{MUSIC}(\theta,\phi,\gamma) = \frac{1}{\mathbf{Y}^H(\theta,\phi,\gamma)\mathbf{V}_Q\mathbf{V}_Q^H\mathbf{Y}(\theta,\phi,\gamma)} \tag{4}$$

where H denotes the matrix Hermitian operation; the column vector $\mathbf{Y}(\theta,\phi,\gamma) = G_\phi(\theta,\phi)\sin(\gamma) + G_\theta(\theta,\phi)\cos(\gamma)$ considers the complex radiation patterns and polarization angles of incoming signals; and the noise-subspace matrix V_Q is obtained from the covariance matrix of v_n in (3).

3. DF ANTENNA ARRAY

3.1. Design of the Top-Hat UTA

As a design example, three top-hat antennas are chosen in the UTA, mounted on a ground plane with a size of $90 \times 90\,\text{cm}^2$ ($1.96\lambda \times 1.96\lambda$), operating at 650 MHz with a wavelength of 46 cm approximately. The ground dimension of $90 \times 90\,\text{cm}^2$ is chosen to consider the future work on platform-based DF arrays. Fig. 3 shows dimensions of the proposed three-element UTA with three design parameters: width w, height h, and element center-to-center separation s. The full-wave numerical simulation software FEKO is used to perform numerous parametric studies, where the optimized wideband antenna array at 650 MHz is achieved with $w = 20$ cm, $h = 23$ cm, and $s = 25$ cm. The corresponding electrical size is $0.34\lambda\times0.34\lambda\times0.39$ based on the wavelength at the lowest operational frequency of 510 MHz. There is no observation of any stability issue on the following DF results.

Figure 4 shows S parameters of the proposed top-hat UTA. The mutual coupling among antenna elements can be observed through S_{12}, S_{13}, and S_{23}, which will influence the DF accuracy. A higher S_{13} across the frequency band from 500 MHz to 800 MHz indicates a stronger mutual coupling between elements 1 and 3. Due to the presence of mutual coupling, the reflection coefficient S_{22} of element 2 is different from S_{11} and S_{33} of elements 1 and 3. The -10 dB frequency bandwidth (BW) of the antennas 1 and 3 is approximately 200.62 MHz with a fractional BW of 32.1% at 650 MHz, and that of the antenna 2 is about 209.79 MHz with a fractional BW of 33.3% at 630 MHz. The wide BW will improve the possibility of signal detections and interceptions. It is also observed that the

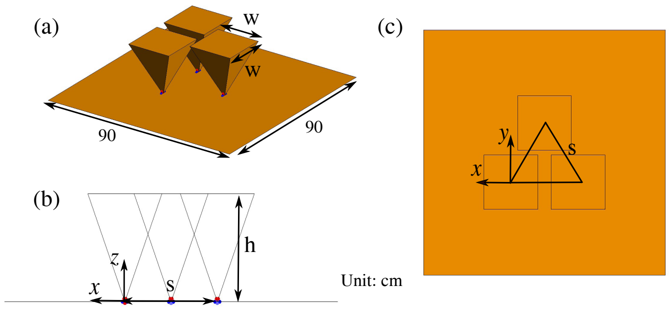

FIGURE 3. The uniform triangular antenna array with $w = 20$ cm, $h = 23$ cm, and $s = 25$ cm, operating at 650 MHz. (a) Three-dimensional view. (b) Side view in xz plane. (c) Top view in xy plane.

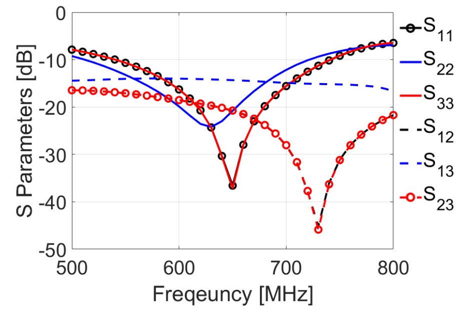

FIGURE 4. S parameters of the three top-hat antennas in the UTA.

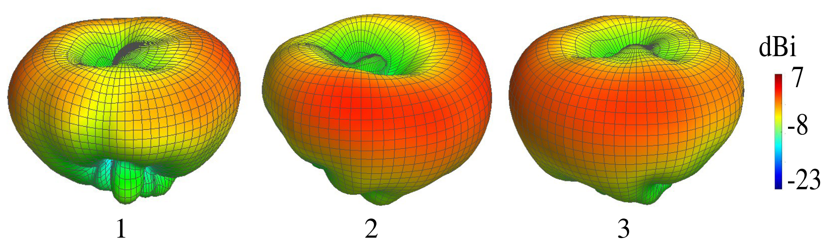

FIGURE 5. The realized gain patterns of the proposed three antenna elements in the UTA.

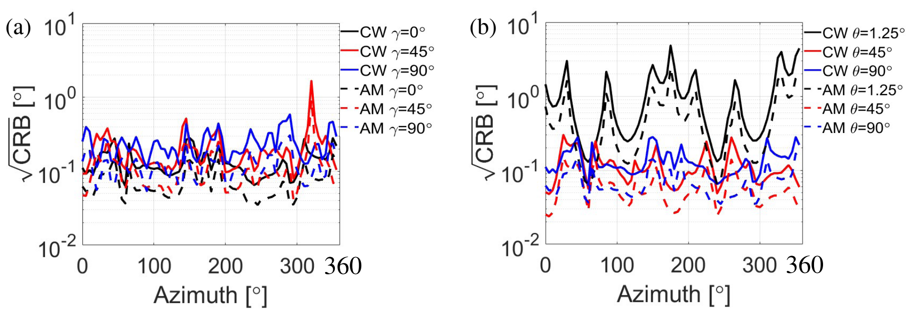

FIGURE 6. Comparison of CRB values based on incident CW and AM signals as a function of azimuth angles at 650 MHz. (a) The elevation angle $\theta = 90^\circ$ with different polarization angles γ. (b) The polarization angle $\gamma = 0^\circ$ with different elevation angles θ. Assume that the snapshot $K = 100$ and SNR $= 25$ dB.

central frequency of antennas 1 and 3 is 650 MHz, and that of antenna 2 is 630 MHz because of mutual coupling. This will not have a great impact on the DF accuracy of the proposed UTA at 650 MHz, since it is within the operational frequency of the antenna 2. Fig. 5 presents the realized gain patterns of the three antenna elements in the UTA. Observe that the radiation patterns of the three identical antennas are different because of mutual coupling, which will be used to demonstrate DF performance in the following subsection. The ϕ and θ components of the complex radiation pattern of the nth element in the UTA are denoted as $G_{n\phi}(\theta, \phi)$ and $G_{n\theta}(\theta, \phi)$, which are implemented to the physics-based MUSIC algorithm in (4).

3.2. DF Performance of the Top-Hat UTA

Figure 6 presents the comparison of physics-based Cramer-Rao bound (CRB) values based on incident CW and AM signals as a function of full azimuth angles from 0° to 360° at 650 MHz, considering the realized gain patterns in Fig. 5. CRB

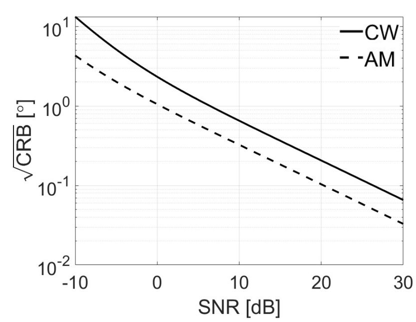

FIGURE 7. Comparison of CRB values based on incident CW and AM signals as a function of SNR at 650 MHz. Assume that the incoming signal has an elevation angle of $\theta = 90^\circ$, an azimuth angle of $\phi = 90^\circ$, and a polarization angle of $\gamma = 0^\circ$. The snapshot number K is 100.

can provide theoretical low bounds of DF accuracies of the proposed three-element UTA, which vary with azimuth, elevation, and polarization angles, snapshot numbers, and signal-

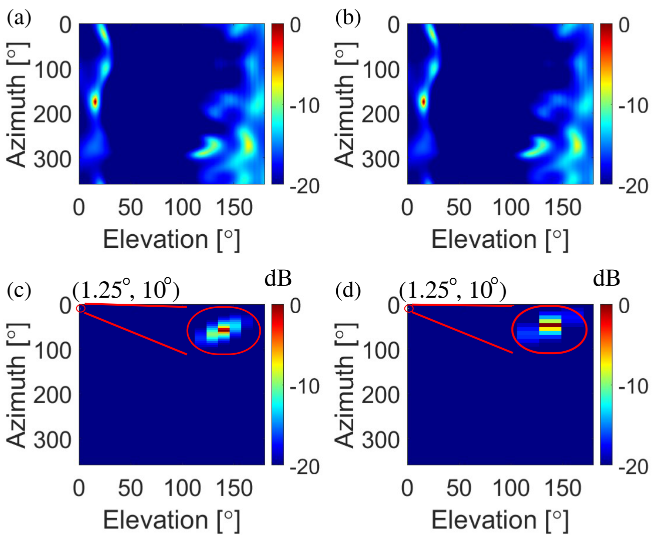

FIGURE 8. 2D MUSIC spectrum of the proposed antenna array receiving incident CW and AM signals from an elevation angle $\theta = 1.25°$, an azimuth angle $\phi = 10°$, and a polarization angle $\gamma = 0°$ with SNR = 25 dB and the snapshot number $K = 100$. (a) CW, array manifold; (b) AM, array manifold; (c) CW, consider modulation; (d) AM, consider modulation. Each inset shows the corresponding zoomed-in estimated DOA (1.25°, 10°).

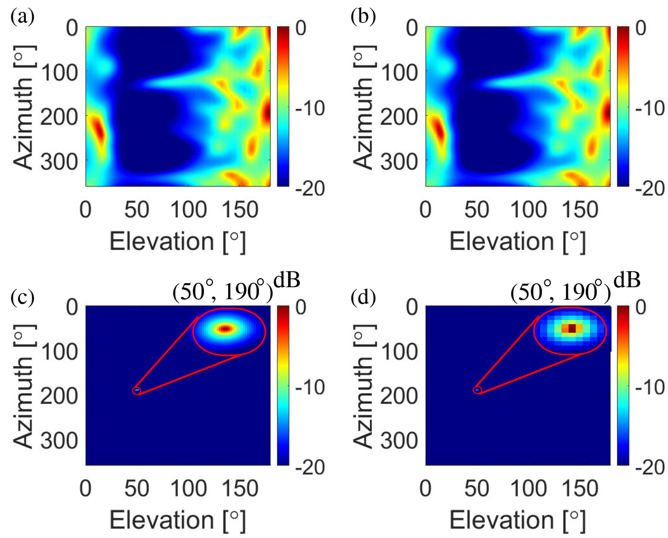

FIGURE 9. 2D MUSIC spectrum of the proposed antenna array receiving incident CW and AM signals from an elevation angle $\theta = 50°$, an azimuth angle $\phi = 190°$, and a polarization angle $\gamma = 0°$ with SNR = 25 dB and the snapshot number $K = 100$. (a) CW, array manifold; (b) AM, array manifold; (c) CW, consider modulation; (d) AM, consider modulation. Each inset shows the corresponding zoomed-in estimated DOA (50°, 190°).

to-noise ratios (SNRs). CRB values can be obtained by taking inverse of the Fisher information matrix of received signals shown in (3), where details can be found in [2, 14]. As depicted in Fig. 1, assume that an incoming linearly polarized plane wave with different elevation and polarization angles is in the far field of the receiving UTA. For incoming CW signals, the carrier frequency $f_c = 650$ MHz, the ϕ component electrical field intensity at the receiver $E_\phi(t) = e^{j2\pi f_c t}\sin(\gamma)$, and the θ component electrical field intensity at the receiver $E_\theta(t) = e^{j2\pi f_c t}\cos(\gamma)$. For incoming AM signals, the modulating frequency $f_m = 20$ kHz, the carrier frequency $f_c = 650$ MHz, the ϕ component electrical field intensity at the receiver $E_\phi(t) = [1 + \cos(2\pi f_m t)]e^{j2\pi f_c t}\sin(\gamma)$, and the θ component electrical field intensity at the receiver $E_\theta(t) = [1 + \cos(2\pi f_m t)]e^{j2\pi f_c t}\cos(\gamma)$. The received signals have an SNR of 25 dB, and the snapshot number is 100 with a sampling time interval of 1 ns.

Figure 6(a) shows CRB comparison based on incident CW and AM signals with a fixed elevation angle of 90° but varying polarization angles of 0°, 45°, and 90°. Observe that precise DOA estimations could be realized with an accuracy better than 0.28°, 1.67°, and 0.59° for incident CW signals and better than 0.17°, 0.93°, and 0.31° for incident AM signals when the polarization angles $\gamma = 0°$, 45°, and 90° respectively. The average CRB values calculated based on the azimuth angles from 0° to 360° and the polarization angles of 0°, 45°, and 90° are 0.20° and 0.10° for incident CW and AM signals, respectively. Fig. 6(b) shows CRB comparison based on incident CW and AM signals with a fixed polarization angle of 90° but varying elevation angles of 1.25°, 45°, and 90°. Due to the null directions along elevation angles of 0° and 180° in the radiation patterns of the three antenna elements in Fig. 5, a high DF accuracy cannot be achieved in these two directions by the proposed top-hat UTA. However, accurate DOA estimations can be realized when the incoming signals are from the elevation angles of 1.25° and 178.75°. Observe that DF accuracies better than 4.86°, 0.30°, and 0.28° for incident CW signals and better than 2.44°, 0.15°, and 0.17° for incident AM signals can be achieved when the elevation angles $\theta = 1.25°$, 45°, and 90° respectively. As expected, DF accuracies will be improved when incoming signals are away from zenith angles. Meanwhile, the CRB variation based on AM signals follows that based on CW signals due to the same phase but different amplitudes between AM and CW signals. The average CRB values calculated based on the azimuth angles from 0° to 360° and the three elevation angles $\theta = 1.25°$, 45°, and 90° are 0.47° and 0.24° for incident CW and AM signals, respectively. This shows that the best achievable DF accuracy for AM signals could be higher than that for CW signals when the polarization angle is 90°. These CRB results demonstrate that the proposed three-element top-hat UTA could provide accurate DOA estimations. The DF accuracy could be further improved by implementing more array elements and increasing the snapshot number.

Figure 7 presents the comparison of CRB values based on incident CW and AM signals as a function of SNR from −10 to 30 dB. Observe that DF accuracies better than 2.33° and 1.05° can be achieved for CW and AM signals when SNR is above 0 dB. To further verify DOA estimation accuracies of the proposed three-element top-hat UTA, Fig. 8 shows 2D MUSIC spectrum as a function of both azimuth and elevation angles based on incident CW and AM signals. Assume that the linearly polarized incoming signal has a polarization angle of $\gamma = 0°$ and elevation and azimuth angles (1.25°, 10°) with SNR = 25 dB and the snapshot number $K = 100$ with a sam-

TABLE 1. Comparisons of DOA accuracies.

Ref.	Array Type	Number of Antennas	Frequency [MHz]	Element Spacing [λ]	Signal Modulation	Snapshot	SNR [dB]	DOA Accuracy [°]
[2]	Linear	6	N/A	0.25	N/A	100	20	2.50
[3]	Linear	10	3000	0.5	N/A	5000	10	0.50
[4]	Linear	10	N/A	N/A	N/A	200	20	0.10
[5]	Linear	14	N/A	0.5	N/A	300	10	0.10
[6]	Circular	8	N/A	N/A	N/A	100	10	0.40
[7]	Linear	4	60000	1	LFM	256	10	10^{-6}
[8]	Linear	5	300	0.5	N/A	1	26	0.20/0.60
[9]	Nonuniform Triangular	3	N/A	0.5, 0.71	LFM	100	20	0.01
[12]	Linear	8	2000	0.5	BPSK	10^5	10	4×10^{-3}
[13]	Distributed	5	10	N/A	CW	100	25	0.60
[14]	N/A	1	625	N/A	CW	100	25	0.15
[15]	N/A	1	21	N/A	CW	100	25	1.06
This Work	Uniform Triangular	3	650	0.42	AM	100	20	0.10

pling time interval of 1 ns. Figs. 8(a) and 8(b) show physics-based 2D MUSIC spectrum without considering the signal variations $e^{j2\pi f_c t}$ for the CW signal and $[1+\cos(2\pi f_m t)]e^{j2\pi f_c t}$ for the AM signal. Observe that the conventional MUSIC algorithm [1] using triangular array manifold provides inaccurate DOA estimations (15.63°, 175°). The similarity in Figs. 8(a) and 8(b) is because the received signals are measured within 100 ns, and CW and AM signals in Fig. 2 are similar within 100 ns in the simulations. Figs. 8(c) and 8(d) present 2D MUSIC spectrum with considering the incident CW and AM signals in the MUSIC algorithm, where precise DOA estimations (1.25°, 10°) are achieved. A priori knowledge of CW and AM signals is assumed.

To validate the DF accuracy with a signal from another direction, Fig. 9 shows 2D MUSIC spectrum of the proposed antenna array receiving incident CW and AM signals from an elevation angle $\theta = 50°$, an azimuth angle $\phi = 190°$, and a polarization angle $\gamma = 0°$ with SNR $= 25$ dB, the snapshot number $K = 100$, and a sampling time interval of 1 ns. Similar to the results in Figs. 8(a) and 8(b), Figs. 9(a) and 9(b) present physics-based 2D MUSIC spectrum without considering the CW and AM signal variations. It is further verified that the traditional MUSIC algorithm fails to provide DOA estimations. An accurate DOA estimation (50°, 190°) is obtained in Figs. 9(c) and 9(d), due to the consideration of the signal modulation. There is no angle ambiguity observed within nearly all field of views from 1.25° to 178.75° in the elevation direction and from 0° to 360° in the azimuth direction. Both CRB calculations and MUSIC spectrum shown in Figs. 6–9 validate DF performance of the proposed UTA in detecting CW and AM signals.

Table 1 shows comparisons of DOA accuracies among the literatures and the proposed work. Observe that the proposed work achieves a better DF accuracy of 0.10° than most antenna arrays [2, 3, 6, 8, 9, 13–15]. The linear arrays in [4, 5] have the same DOA accuracy of 0.10° as the proposed triangular array. However, more than three antenna elements are applied, and practical antennas are not considered. The linear arrays in [7, 12] and the nonuniform triangular array in [9] provide better DOA accuracies than the proposed work. However, compared to the proposed array, more antenna elements and snapshot numbers are implemented in [7, 12], and practical antennas are not considered in [7]. For the nonuniform triangular array in [9], the number of antennas, snapshot numbers, and SNR values are the same. Although a DOA accuracy of 0.01° can be achieved by the nonuniform triangular array detecting an LFM signal, the practical antenna array with the presence of mutual coupling is not considered. The proposed triangular array is more compact with an element spacing of 0.42λ, demonstrating that strong mutual coupling will not affect the DF accuracy with the consideration of antenna radiation patterns.

4. CONCLUSIONS

Unlike traditional DF arrays, the complex radiation patterns are considered in physics-based CRB calculations and MUSIC spectrum. Unlike conventional array elements using linear wire antennas, the wideband top-hat antennas are implemented to increase the probability of signal detections. Instead of assuming constant amplitude of incident signals, realistic CW and AM incoming waves are investigated. Accurate DOA estimations using the proposed three-element-top-hat UTA are demonstrated by calculating CRB values with different elevation, azimuth, and polarization angles. 2D DF capability of the antenna array with a wide field of view from 1.25° to 178.75° in the elevation direction and from 0° to 360° in the azimuth direction is validated by the MUSIC algorithm, where no angle ambiguity is observed.

REFERENCES

[1] Ferrara, E. and T. Parks, "Direction finding with an array of antennas having diverse polarizations," *IEEE Transactions on Antennas and Propagation*, Vol. 31, No. 2, 231–236, 1983.

[2] Weiss, A. J. and B. Friedlander, "Performance analysis of diversely polarized antenna arrays," *IEEE Transactions on Signal Processing*, Vol. 39, No. 7, 1589–1603, 1991.

[3] Liao, B. and S.-C. Chan, "A cumulant-based method for direction finding in uniform linear arrays with mutual coupling," *IEEE Antennas and Wireless Propagation Letters*, Vol. 13, 1717–1720, 2014.

[4] Wang, Q., T. Dou, H. Chen, W. Yan, and W. Liu, "Effective block sparse representation algorithm for DOA estimation with unknown mutual coupling," *IEEE Communications Letters*, Vol. 21, No. 12, 2622–2625, Dec. 2017.

[5] Zhang, X., T. Jiang, Y. Li, and Y. Zakharov, "A novel block sparse reconstruction method for DOA estimation with unknown mutual coupling," *IEEE Communications Letters*, Vol. 23, No. 10, 1845–1848, Oct. 2019.

[6] Hu, W. and Q. Wang, "DOA estimation for UCA in the presence of mutual coupling via error model equivalence," *IEEE Wireless Communications Letters*, Vol. 9, No. 1, 121–124, Jan. 2020.

[7] Xu, Z., Y. Chen, and P. Zhang, "A sparse uniform linear array DOA estimation algorithm for FMCW radar," *IEEE Signal Processing Letters*, Vol. 30, 823–827, 2023.

[8] Hwang, S., S. Burintramart, T. K. Sarkar, and S. R. Best, "Direction of arrival (DOA) estimation using electrically small tuned dipole antennas," *IEEE Transactions on Antennas and Propagation*, Vol. 54, No. 11, 3292–3301, 2006.

[9] Yuan, X., "Direction-finding wideband linear FM sources with triangular arrays," *IEEE Transactions on Aerospace and Electronic Systems*, Vol. 48, No. 3, 2416–2425, 2012.

[10] Wang, T., B. P. Ng, and M. H. Er, "DOA estimation of amplitude modulated signals with less array sensors than sources," in *2012 IEEE International Conference on Acoustics, Speech and Signal Processing (ICASSP)*, 2565–2568, Kyoto, Japan, Mar. 2012.

[11] Sharif, W., P. Heidenreich, and A. M. Zoubir, "Robust direction-of-arrival estimation for FM sources in the presence of impulsive noise," in *2010 IEEE International Conference on Acoustics, Speech and Signal Processing*, 3662–3665, Dallas, TX, USA, Mar. 2010.

[12] Ni, G., C. He, J. Chen, L. Bai, and R. Jin, "Direction finding and performance analysis with 1 bit time modulated array," *IEEE Transactions on Antennas and Propagation*, Vol. 69, No. 10, 6881–6893, Oct. 2021.

[13] Ren, K., R. Ma, and N. Behdad, "Performance-enhancement of platform-based, HF direction-finding systems using dynamic mode selection," *IEEE Open Journal of Antennas and Propagation*, Vol. 2, 793–806, 2021.

[14] Ren, K., "Direction finding using a single antenna with blade modulation," *IEEE Antennas and Wireless Propagation Letters*, Vol. 21, No. 5, 873–877, May 2022.

[15] Ren, K., "Helicopter-mounted HF direction-finding antenna with rotor-blade modulation using the characteristic mode theory," *IEEE Antennas and Wireless Propagation Letters*, Vol. 22, No. 7, 1597–1601, Jul. 2023.